

REMOTE SENSING
TOOLS
FOR BIOGEOCHEMISTRY

Mary-Elena Carr

Jet Propulsion Laboratory
California Institute of Technology

Acknowledgements

All PPARR3 participants (list of groups follows) for their hard work.

Goddard DAAC, SeaWiFS Project for providing SST, chlorophyll and PAR data; JPL-PODAAC and NASA's Pathfinder Program (F. Wentz) for wind speed data; T. Takahashi (LDEO) for Δp_{CO_2} data.

This research was carried out at the Jet Propulsion Laboratory, California Institute of Technology, under a contract with the National Aeronautics and Space Administration.

OCEAN BIOGEOCHEMISTRY:

THE CARBON CYCLE

On a global basis, the ocean is a sink of atmospheric CO_2 , although there are large regions which outgas to the atmosphere.

Atmospheric CO_2 varies more from year to year than the rate of emission. The variability of uptake by the ocean is not well known.

CO_2 is fixed by photosynthesis, or primary production (PP) into organic matter.

Photosynthesis on land and in the ocean is a major term of the global carbon budget through its influence on atmospheric CO_2 .

New production is the oceanic PP fueled by nutrients originating outside the illuminated upper layer.

Steady state requires that the uptake of new nutrients be balanced by the export of carbon from the upper layer (Eppley and Peterson 1979).

REMOTE SENSING CAPABILITIES

Great for spatio-temporal coverage and consistency of methodology.

Limited by what they can measure and depth of penetration and resolution.

- Sea surface temperature (SST): AVHRR, MODIS. TRMM sees through clouds; limited to $\pm 40^\circ$.
- (To be launched in 2006) Sea Surface Salinity
- Sea surface height (SSH): Topex/POSEIDON (T/P) and JASON.
- Wind speed and direction : QuikScat (since June 1999), SSM/I, SeaWinds (launched 15 Dec).
- Chlorophyll concentration : SeaWiFS, MODIS.

WHAT DO WE NEED TO KNOW?

Exchange of CO_2 between ocean and atmosphere:

pCO_2 of the ocean: SST, Salinity, [chl]

Gas exchange coefficient: wind, surface roughness

Photosynthesis: color, SST, irradiance, fluorescence

New or export production:

Supply of nutrients: heat flux, precipitation

Nutrient uptake: heat flux, heat storage, SST

f-ratio: SST, PP, [NO_3], [chl]

Functional types: optical or compound remote sensing

Partitioning and conversion of carbon species: reflectance

Biological production of radiatively active gases: reflectance, irradiance

Atmospheric aerosol patterns: reflectance

Variability and unresolved process:

Eddies : (T/P)

Coastal processes : Geostationary platforms, multi-spectral reflectance

HOW DO WE USE SATELLITE OBSERVATIONS?

1. Derive relationship between *in situ* variable(s) of interest and remotely-sensed variable(s).
2. Apply relationship to maps of remotely-sensed variable(s).

Errors arise because the relationship

is poorly constrained.

does not hold everywhere or always.

Three examples of approaches which use remote sensing to improve our understanding of a major flux term:

Air-sea exchange of CO_2

Primary production from ocean color: a comparison of algorithms

New production from heat storage (T/P)

CONCLUSIONS

- Satellite data are not perfect nor complete.

Though the standard products of most sensors are of high quality (in most places), compound products (such as PP, new production, functional type, etc.) should not be taken at face value.

- Emphasis must be placed on satellite observations concurrently with field programs.

- Satellites uniquely provide

best spatio-temporal coverage (extrapolation)

context for oceanographic processes

data to force, assimilate into, constrain models

estimate of inaccessible scales of variability

- The sea-going community must request new and improved sensors, such as salinity.

Example 1:
CO₂ EXCHANGE COEFFICIENTS
FROM SSM/I AND QUIKSCAT

with W. Tang and W.T. Liu (JPL)

MOTIVATION

Space-borne wind speed sensors measure winds over the world ocean in ~ 2 days. This unprecedented coverage allows us to calculate variability on a range of temporal scales.

Our ultimate goal is to construct high quality long-term global time series of K , the exchange coefficient for CO₂.

APPROACH

The Special Sensing Microwave Imager (SSM/I) estimates wind speed from the microwave brightness temperature. There have been a series of identical sensors flying on the DMSP platform since 1988.

SeaWinds on QuikSCAT, a Ku-band scatterometer, measures wind speed and direction. It has been providing data since July of 1999.

The data quality of SSM/I is inferior to that of scatterometers, which additionally provide the wind direction. But, we have 13 years of daily global maps and the opportunity to address interannual variability is attractive.

To address the quality of SSM/I for this goal we compare here the exchange coefficient and flux derived with SSM/I and with QuikScat for 2000, focusing on January, April, July.

We use the Wanninkhof (1992) parameterization to derive the exchange coefficient, K , in $10^{-2} \text{mol m}^{-2} \text{y}^{-1} \mu\text{atm}^{-1}$

$$K = k_{ave}s \quad (1)$$

where:

s , the solubility, is a $f(\text{SST}, S)$

k_{ave} is the gas transfer velocity estimated

with quadratic dependence on the long-term average wind, u_{ave}

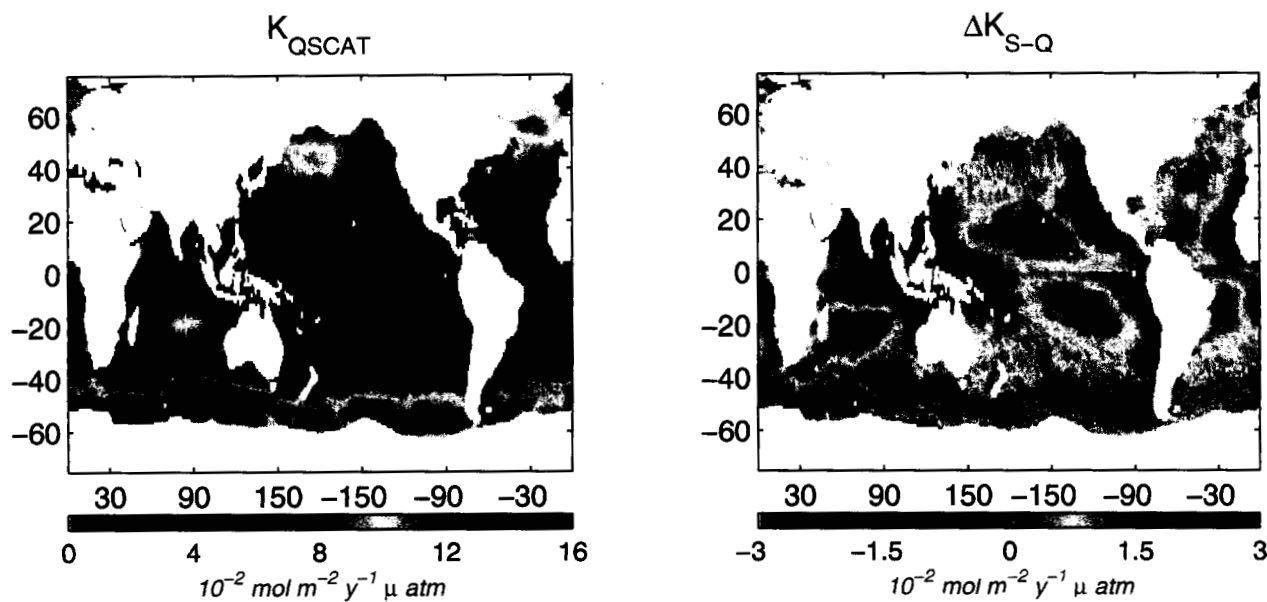
and the Schmidt number, which is a $f(\text{SST})$.

We use monthly mean concurrent SST from Reynolds (1994), wind speeds from SSM/I and QuikSCAT, and climatological salinity from Levitus (1998).

SPATIAL COMPARISON OF K

Maxima around 50° (westerlies) and at $15\text{-}20^\circ$ (trades).

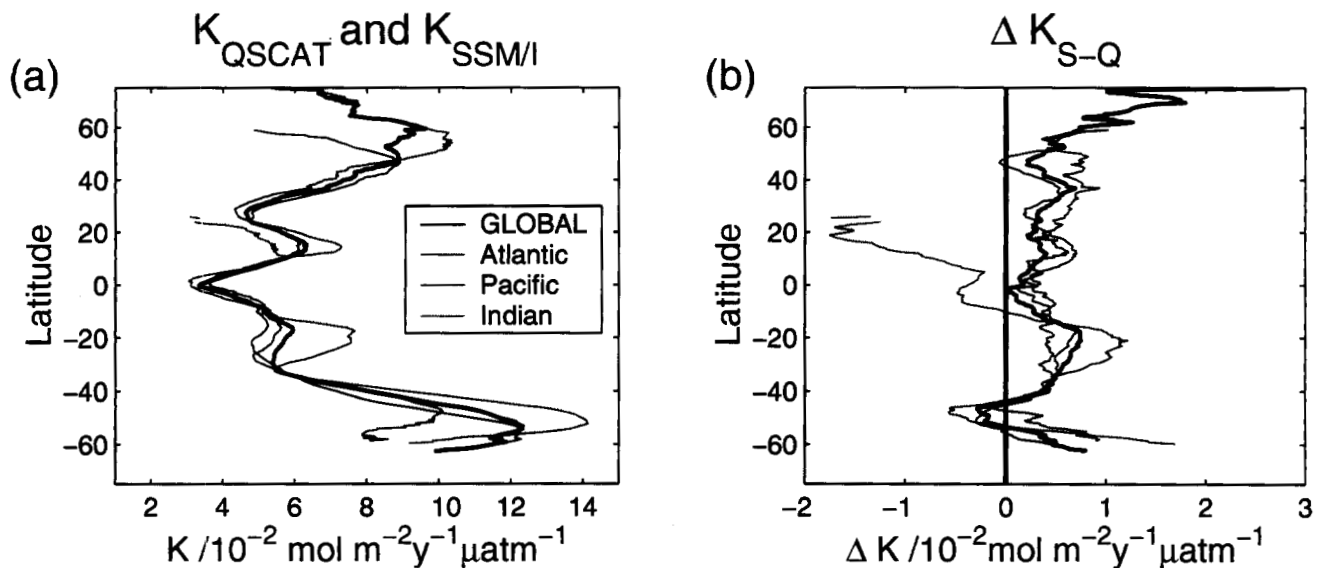
SSM/I generally overestimates K ; negative ΔK in the Eastern Boundary Currents, W Indian Ocean, Arabian Sea, and along 50°S .



$>80\%$ ΔK : $\pm 1.5 \cdot 10^{-2} \text{ mol m}^{-2} \text{ y}^{-1} \mu \text{ atm}^{-1}$

ZONAL MEAN COMPARISON OF K

Maxima correspond to westerly and trade wind bands.



Zonal mean K_S are consistently larger, except at $\sim 50^\circ\text{S}$ and Indian Ocean.

ΔK are less $1 \cdot 10^{-2} \text{ mol m}^{-2} \text{ y}^{-1} \mu\text{atm}^{-1}$ within $\pm 50^\circ$ except in the Indian Ocean.

The two sensors differ least within 5° of 0° .

GLOBAL COMPARISON OF K

ΔK is between 0.16 and $0.6 \cdot 10^{-2} \text{ mol m}^{-2} \text{ y}^{-1} \mu\text{atm}^{-1}$ (2-7%).

Seasonal cycle in the global mean is negligible.

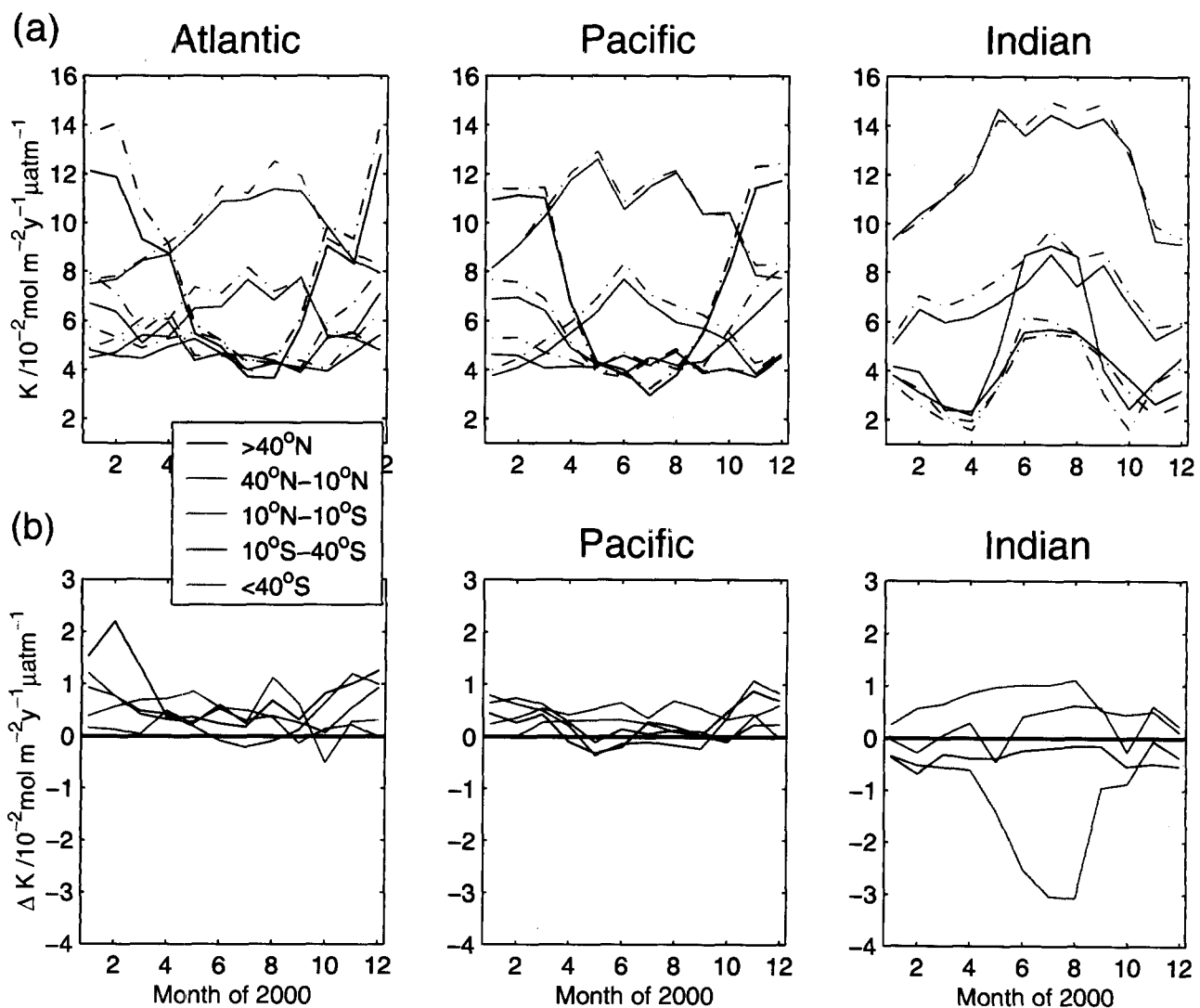
Table 1. Comparison of global mean K_Q and K_S (in $10^{-2} \text{ mol m}^{-2} \text{ y}^{-1} \mu\text{atm}^{-1}$).

	K_Q	K_S	ΔK_{S-Q}
MEAN 00	7.07	7.41	0.34
JAN 00	6.83	7.27	0.44
APR 00	7.17	7.53	0.36
JUL 00	7.42	7.65	0.23
OCT 00	6.98	7.15	0.17

SEASONAL PATTERNS OF K

The amplitude of the seasonal cycle is maximum poleward of 40° .

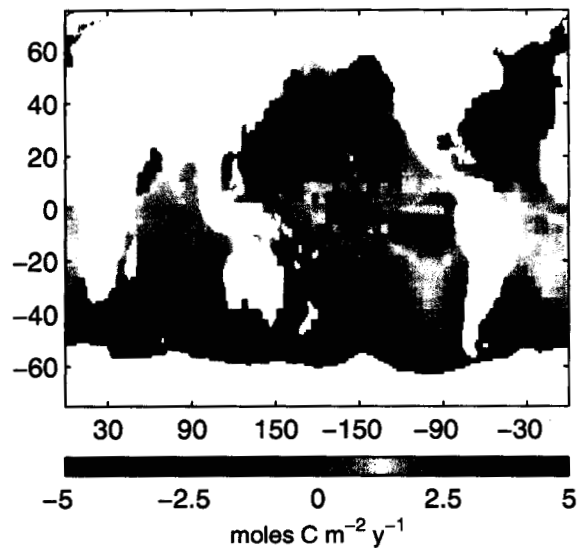
ΔK follows the seasonal cycle and is >0 , except in the equatorial and northern Indian Ocean.



AIR-SEA CO₂ FLUX: MEAN

The air-sea flux of CO₂ was estimated with the monthly mean K for 2000 and climatological maps of $\Delta p\text{CO}_2$ (Takahashi 1999).

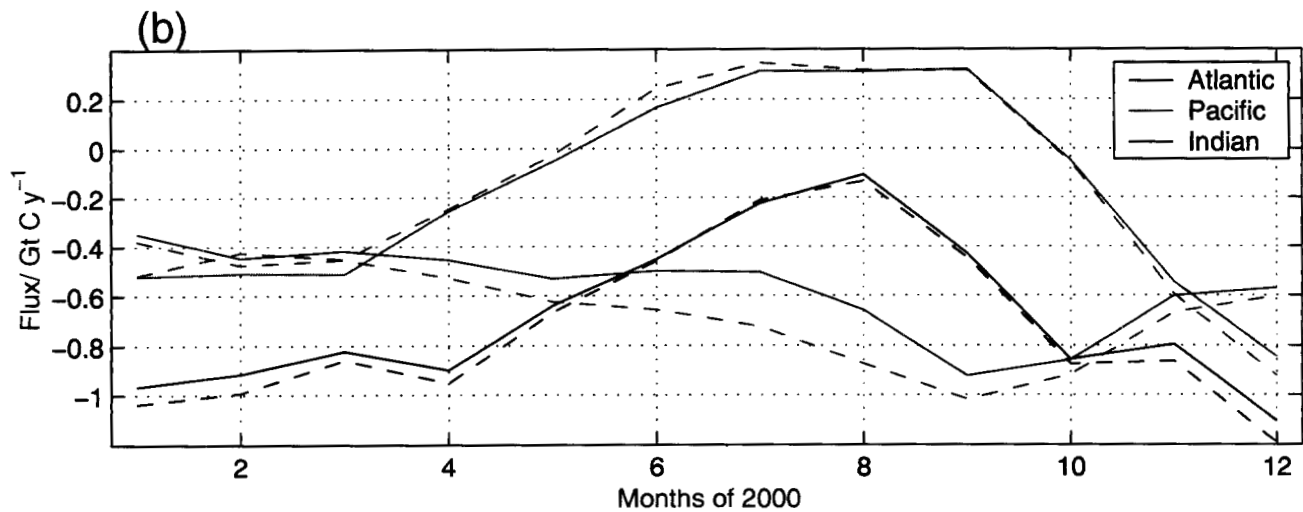
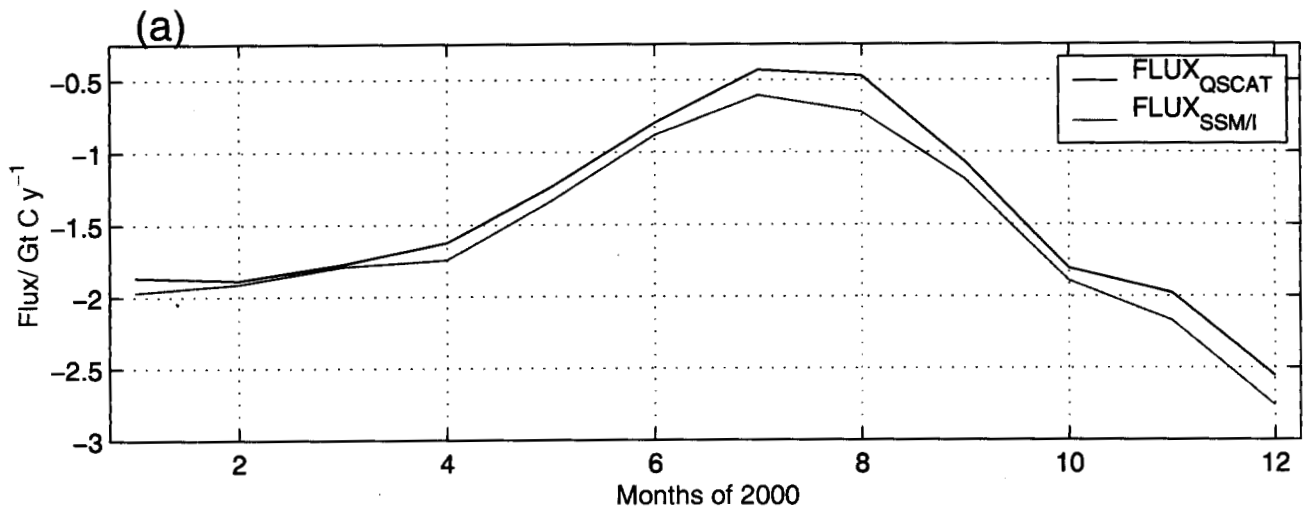
The global flux distribution falls along three bands: poleward of 20° or 30° the ocean is generally a sink of CO₂ (flux is negative) while in the central equatorial band CO₂ goes into the atmosphere (flux is positive).



SSM/I consistently overestimates K and consequently global uptake by 0.09 to 0.18 GtC y^{-1} . This is $\sim 10\%$ except in July and August (41 and 53%).

	JAN	JUL
Flux	-1.86 -1.97	-0.43 -0.61
ΔF	-0.10	-0.18
Area	298	288
Mean flux	-0.76 -0.81	-0.35 -0.40
Mean K	6.75 7.24	7.20 7.50

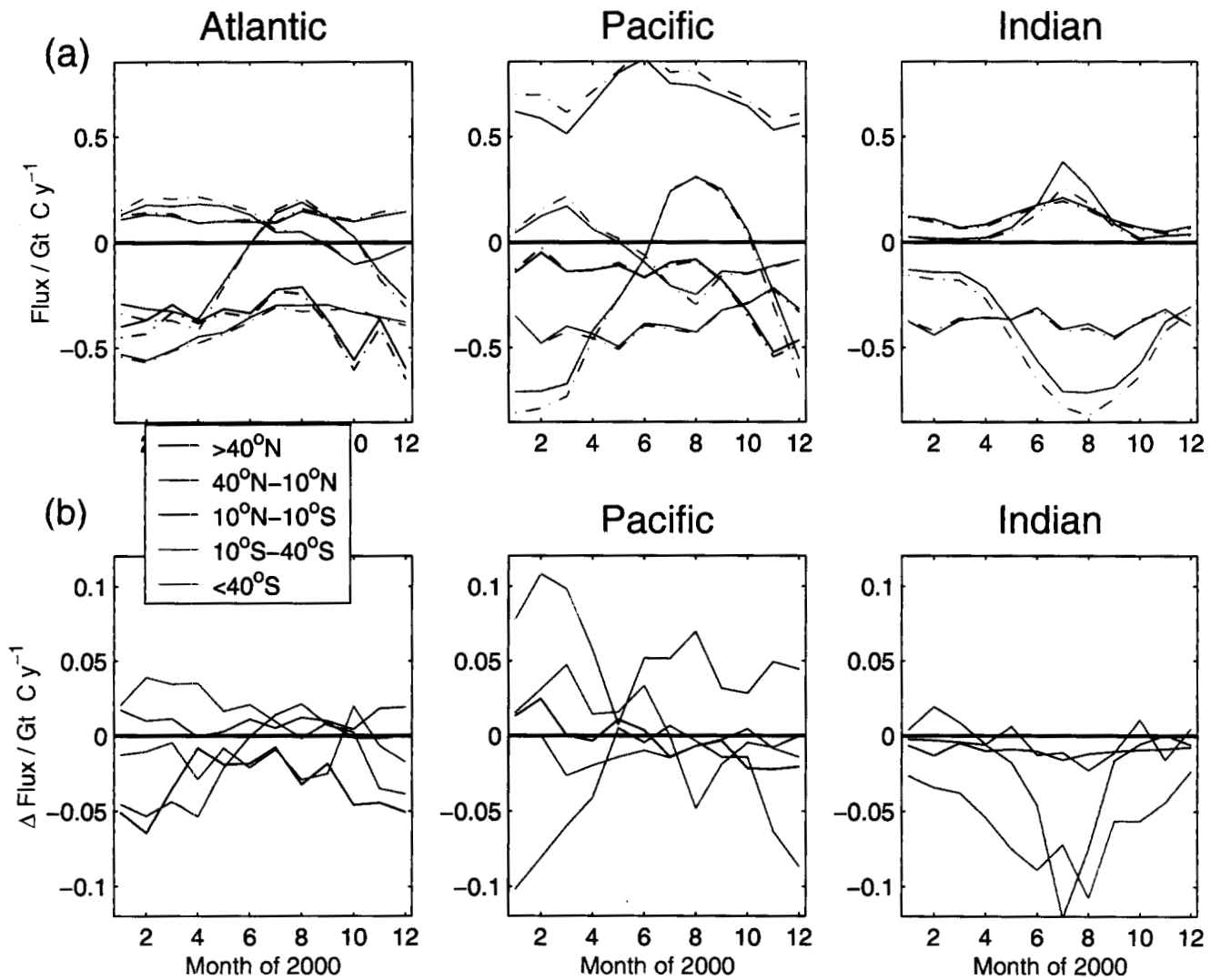
The greatest ΔF occurs in boreal summer in the Indian Ocean when SSM/I underestimates the source in the Arabian Sea and overestimates the uptake in the South Indian, both contributing to an increased sink.



SEASONAL CYCLE OF FLUX

The equatorial regions are a source (Pacific!).

Consistent uptake occurs poleward of 40°S.



ΔK is such that the flux is compensated except in the Indian Ocean ΔK changes sign with the $\Delta p\text{CO}_2$, leading to an overestimate of the carbon flux into the ocean.

CONCLUSIONS EXAMPLE 1

The two sensors see the same general trends but SSM/I tends to overestimate K .

This translates into errors of about $0.4 \cdot 10^{-2} \text{ mol m}^{-2} \text{ y}^{-1} \mu\text{atm}^{-1}$ in zonal and global means and of up to $2 \cdot 10^{-2} \text{ mol m}^{-2} \text{ y}^{-1} \mu\text{atm}^{-1}$ in seasonal variability for meridional bands.

The maximum discrepancy between the two sensors is in the Indian Ocean, where ΔK changes sign with $\Delta p\text{CO}_2$ leading to net overestimate of oceanic uptake.

The uncertainty in global flux from using SSM/I is order 0.15 GtC y^{-1} , thus validating its use to assess variability in flux.

Example 2:

*PRIMARY PRODUCTION ALGORITHM
ROUND-ROBIN 3 (PPARR3)*

with M. Friedrichs (ODU)

MOTIVATION

In PPARR2, a blind intercomparison to *in situ* data the best performing algorithms were within a factor of two. The equatorial Pacific and Southern Ocean data presented higher biases.

Our goal is to provide a framework to systematically compare algorithms which estimate primary production from ocean color.

PPARR3: OUR APPROACH

PART 1. Annual cycle (1998). *Model output inter-comparison.*

PART 2. Sensitivity analysis exploring biomass determination and parameterization of light utilization and photo-adaptive physiology. *Model intercomparison at different stages of PP estimation.*

PART 3. Comparison to in-situ ^{14}C -uptake (ClimPP: 1022 tropical Pacific stations and all JGOFS measurements). *Ground-truth comparison.*

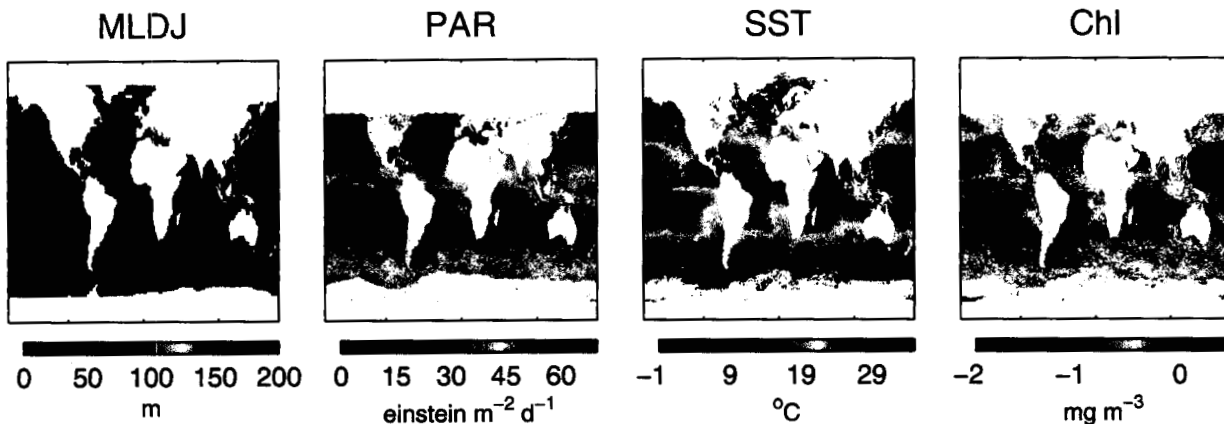
- 1'. David. IPCF. D. Antoine, B. Gentili and A. Morel.
2. Nick. BIO variant. N. Hoepffner and F. Melin.
3. Kirk. K. Waters and B. Bidigare.
4. Tim. Modified IPCF. T. Smyth and S. Groom.
5. Tasha. Arrigo. T. Reddy and K. Arrigo
6. Mike. VGPM. M. Behrenfeld.
7. Mike2. VGPM (Eppley P_{Bopt}). M. Behrenfeld.
8. ModisBF. VGPM. K. Turpie and W. Esaias.
9. Aurea. VGPM. A. Ciotti.
10. Joji. J. Ishizaka and Mr. Kameda.
11. Keith. K. Moore.
12. Heidi. Southern Ocean. H. Dierssen.
13. Heidi2. Southern Ocean chlorophyll. H. Dierssen.
14. Ichio. I. Asanuma.
15. Mark: Province-based. M. Dowell.
- 16'. ModisHYR. HoYoRy. K. Turpie and W. Esaias.
- 17'. RyYo. HoYoRy variant. J. Ryan.
18. HYRZe. HoYoRy variant (Z_e). M-E Carr.
19. Michele. Neural network. M. Scardi.
20. John. J. Marra.
21. SteveB. Hybrid WIM. VGPM P_{Bopt} . S. Lohrenz.
22. SteveB2. Hybrid WIM, VGPM P_{Bopt} . S. Lohrenz.
23. SteveA. Hybrid WIM, IPCF P_{Bmax} . S. Lohrenz.

24. OliCor. Ecosystem model. O. Aumont.
- 25'. KeithE. Ecosystem model. K. Moore.
- 26'. Yasu. Ecosystem model. Y. Yamanaka.
- 27'. Dunne. Restoring GCM. J.Dunne et al.

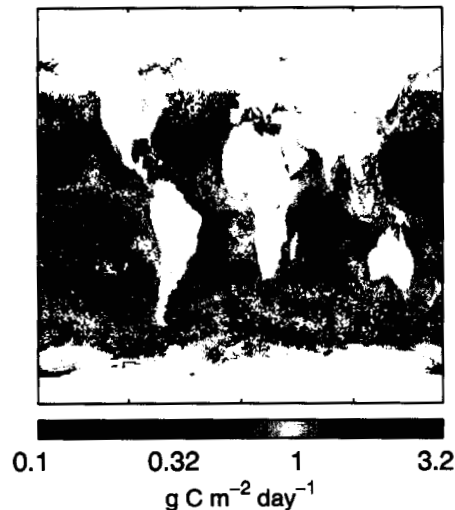
APPROACH

Given identical input files (monthly mean)

Participants return integrated primary production.



MEAN MODELED PP, 24 MODELS



Model spread quantified as a function of 'mean'

standard deviation of mean (\bar{x}) as percentage

$\log_{10}(x_i) - \overline{\log_{10}(x)}$, is equivalent to 'factor of'.

GLOBAL PRODUCTION

Mean global production for 1998 is 51.8 Gt C y^{-1} .

Standard deviation of the mean is 11.7 Gt C y^{-1} (23%)

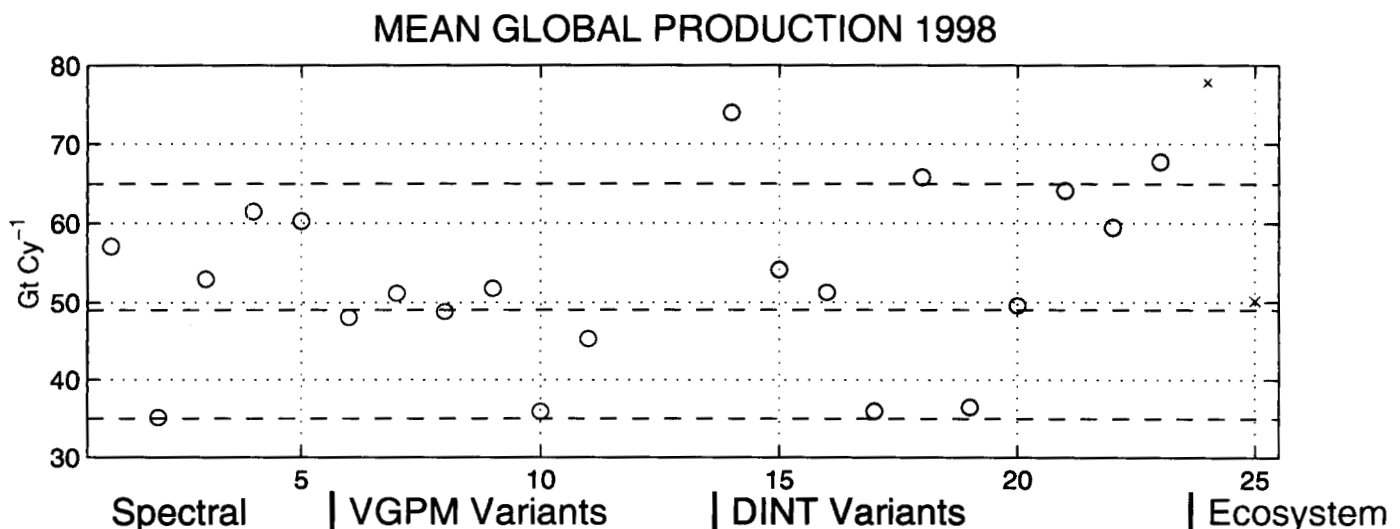
Range of model estimates is 40 Gt C y^{-1} .

LOW: $\sim 35 \text{ Gt C y}^{-1}$ (5 models)

HIGH: $\sim 65 \text{ Gt C y}^{-1}$ (5-7 models, +1E)

INTERMEDIATE: $\sim 49 \text{ Gt C y}^{-1}$ (9 models, +1E)

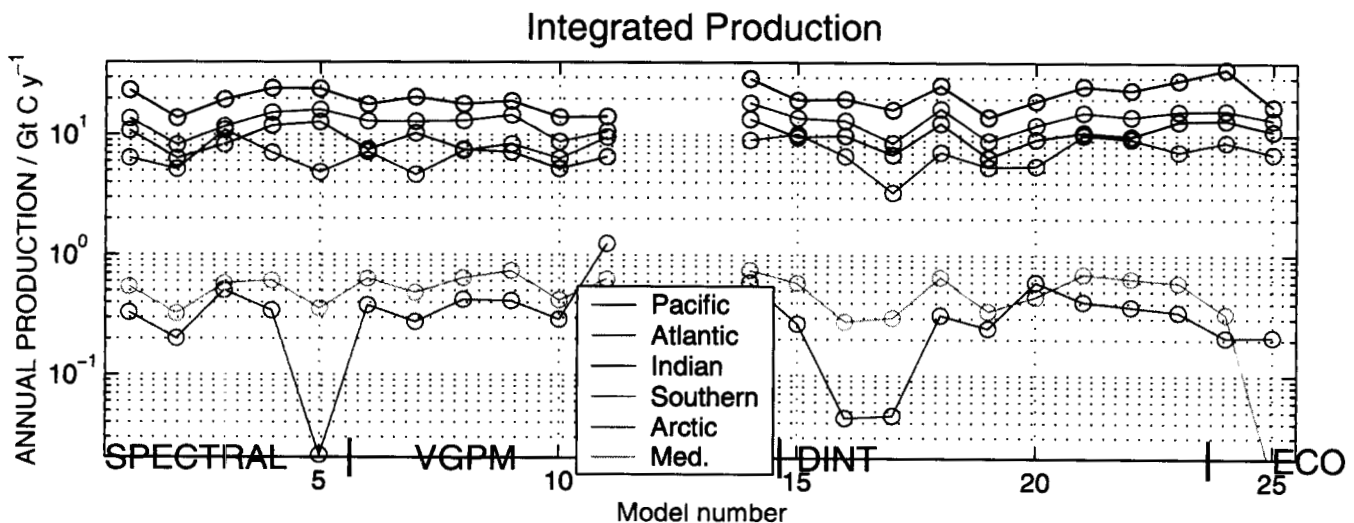
No VGPM variant is in the high level. 1-3 models of each kind are found in the low level (no ecosystem).



BREAKOUT BY BASINS

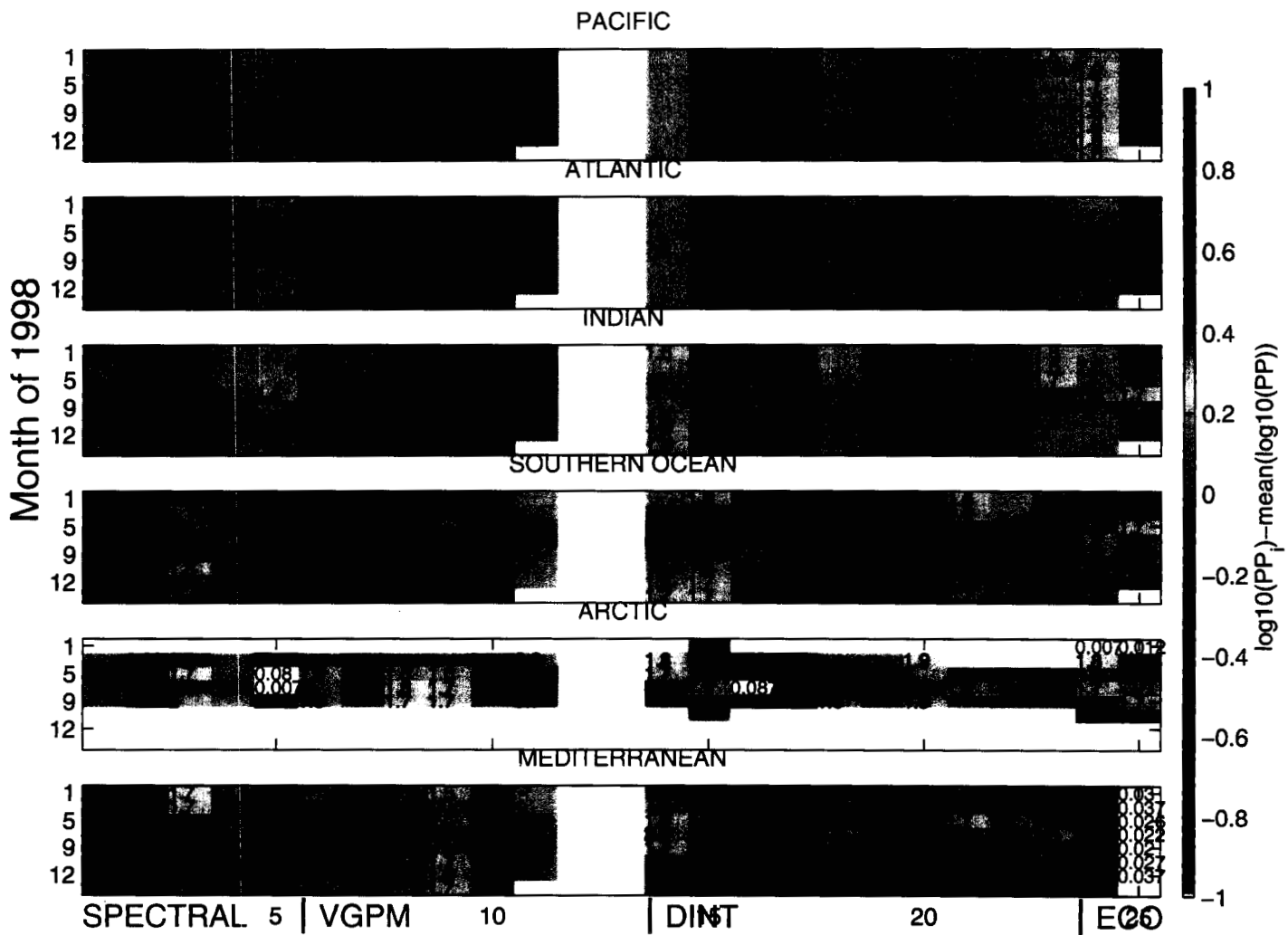
BASIN	AREA	MEAN (%)	MIN	MAX
	%	Gt C y ⁻¹		
Pacific	42	20.7 (40.1)	13.8	29.5
Atlantic	21	12.9 (24.9)	8.2	18.5
Indian	14	9.5 (18.4)	5.2	13.6
Southern	22	7.9 (15.2)	3.3	10.9
Arctic	1.1	0.24 (0.47)	0	1.2
Med.	0.8	0.52 (1)	0.3	0.7

Variability in model estimates is greatest in small basins, and in the Southern Ocean.



There are 2 or 3 'anomalous' models in the Pacific and Atlantic, and 3-5 in the Indian.

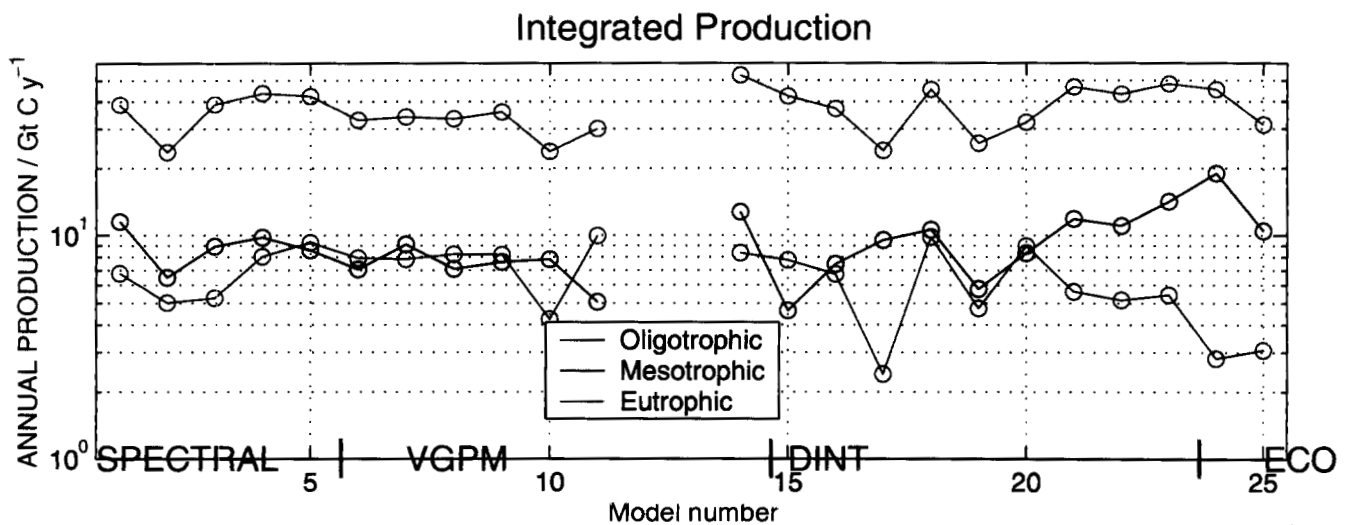
There are 7 anomalous models in the Southern Ocean. Some counter (#2 or 15) the seasonal cycle and some reinforce it (#3 or 5).



CONCENTRATION LEVEL

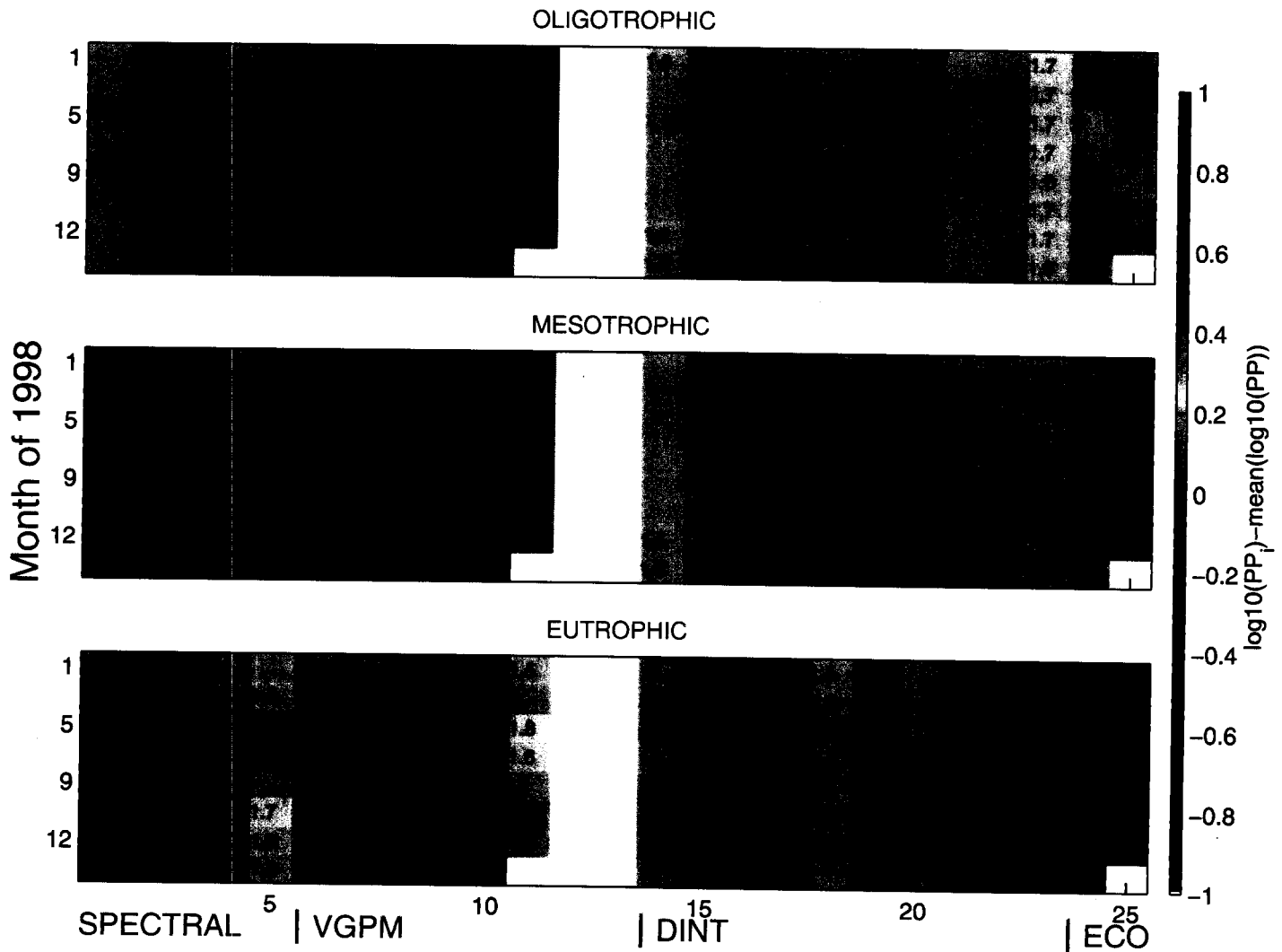
LEVEL	AREA	MEAN (%)	MIN	MAX
	%	Gt C y ⁻¹		
Oligotrophic	~30	8.8 (16.5)	4.6	14.2
Mesotrophic	~65	37.6 (70.5)	23.6	52.9
Eutrophic	3-5	6.9 (12.9)	2.4	9.9

Models vary in relative importance of eutrophic and oligotrophic waters (note spectral and ecosystem models and #16).



The greatest discrepancy is in oligotrophic and eutrophic waters (~ 5 models).

Though less anomalous, there is a tendency to underestimate production in mesotrophic waters.

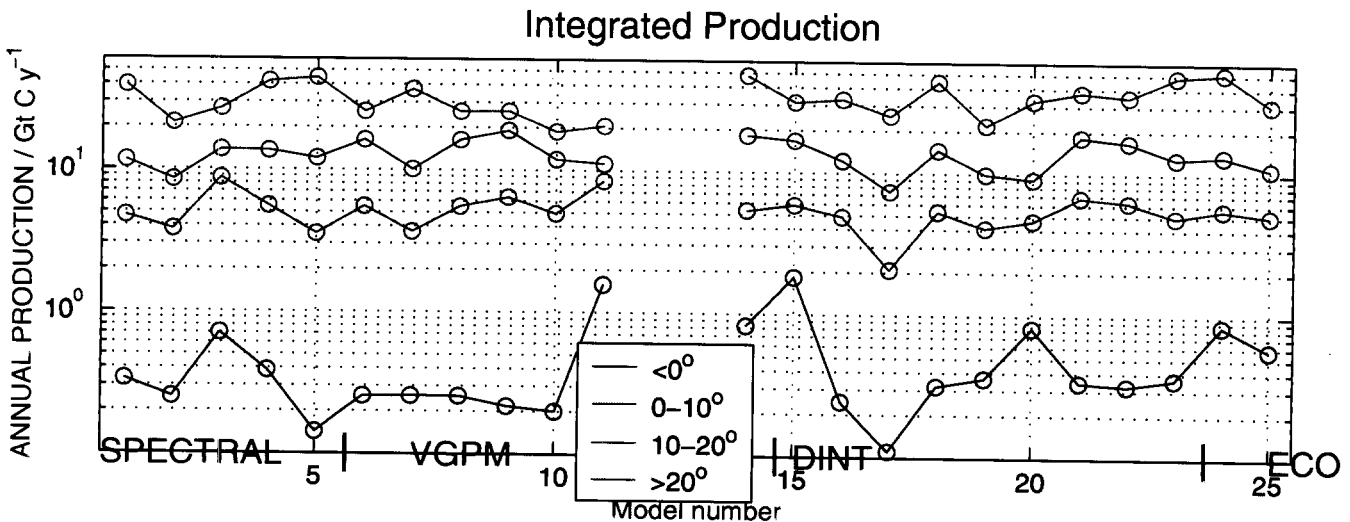


SST BINS

SST RANGE	AREA	MEAN (%)	MIN	MAX
	%	Gt C y ⁻¹		
SST < 0°C	2-4	0.6 (1.2)	0.1	1.8
0° – 10°C	13-17	5.4 (10.2)	2.1	8.7
10° – 20°C	~20	13.5 (25.6)	7.4	18.9
> 20°C SST	~60	33.1 (62.9)	18.8	48.5

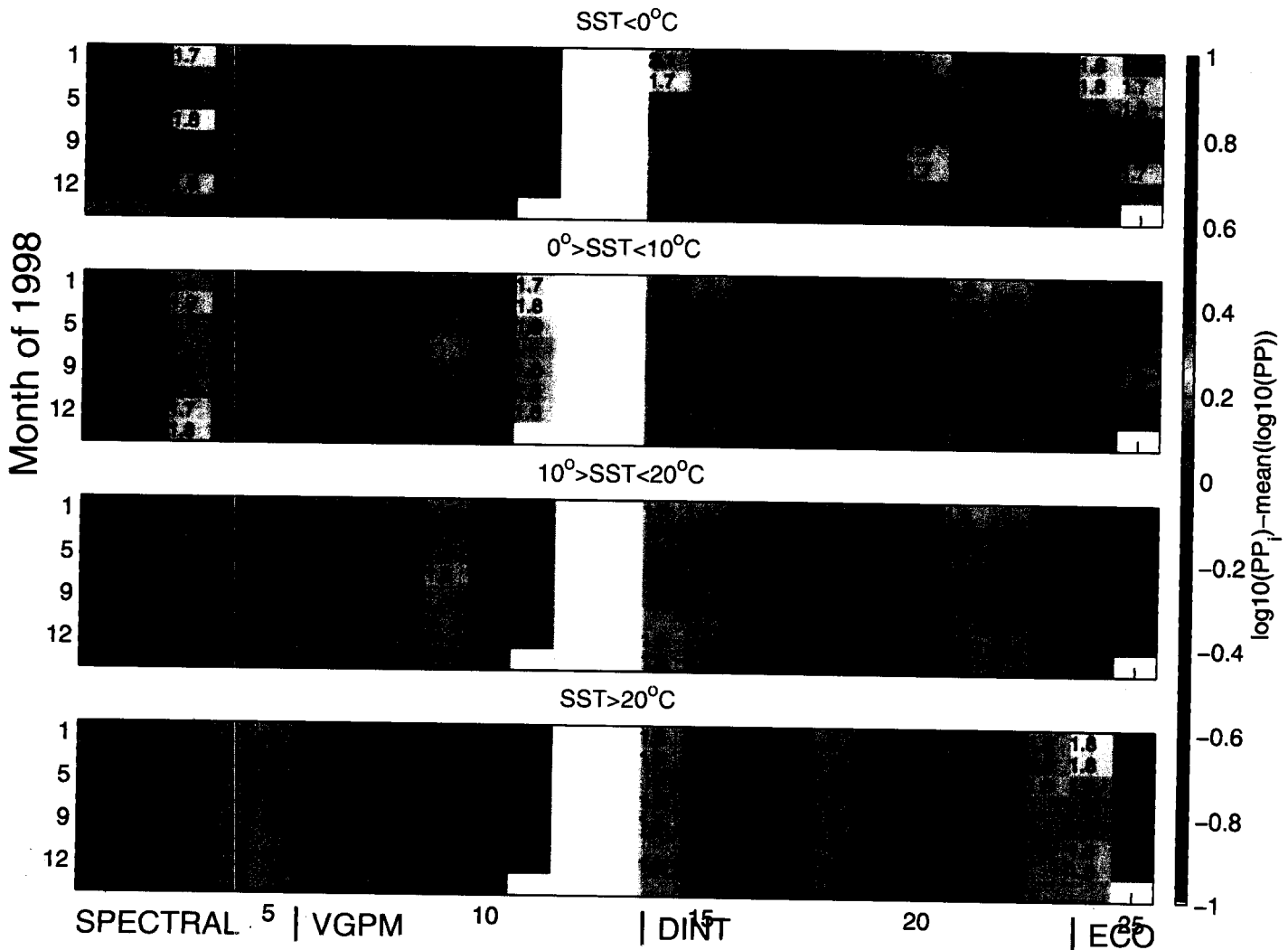
The models are very disparate at SST < 0°C.

VGPM variants appear less sensitive to SST > 0.



Modeled PP in sub-zero waters is very poorly constrained.

A few models are uniformly high/low for $SST > 20^{\circ}C$. Model #17 is low for $SST < 20^{\circ}C$.



REGIONAL PRODUCTION IN THE SOUTHERN OCEAN

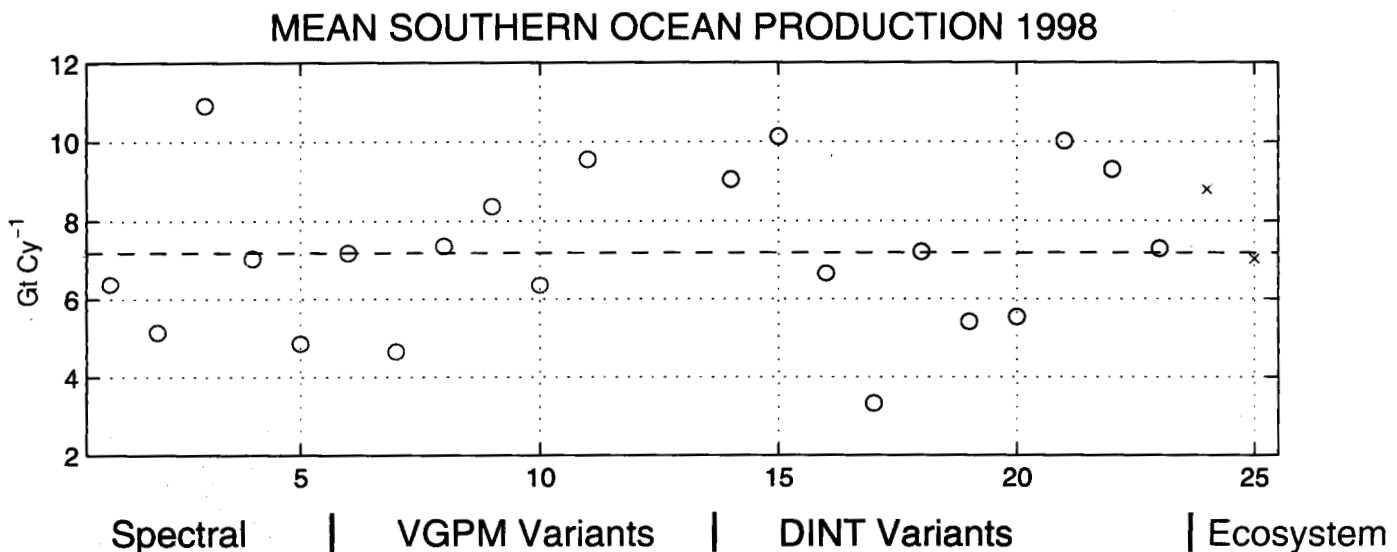
The uncertainty of the role of the Southern Ocean in the carbon cycle is aggravated by the difficulties of field sampling.

There is a disagreement between *in-situ* and satellite-based estimates of production.

Mean production ($<40^{\circ}\text{S}$) for 1998 is 7.2 Gt C y^{-1} .

Standard deviation of the mean is 2 Gt C y^{-1} (30%)

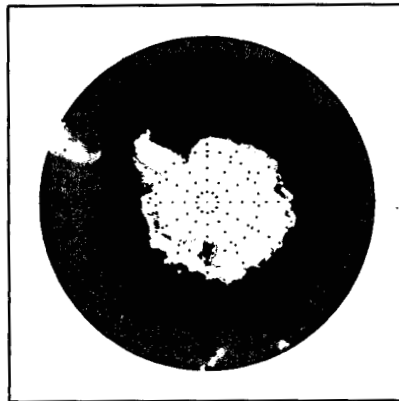
Range of model estimates is 8 Gt C y^{-1} , comparable to the seasonal range for most models.



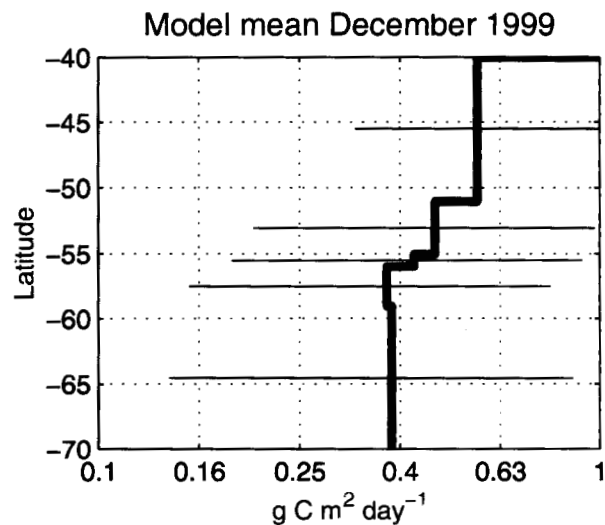
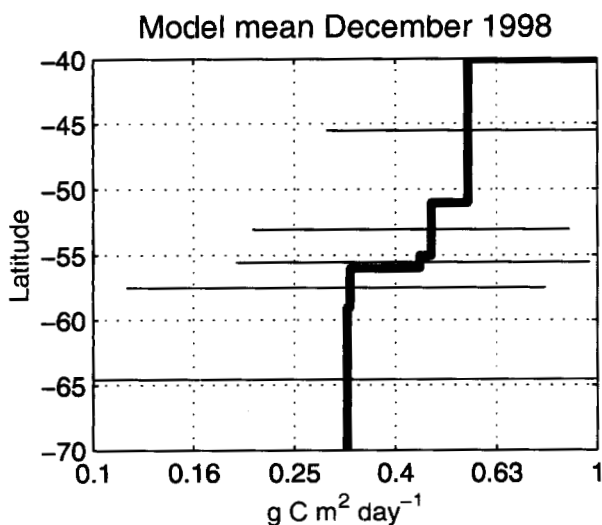
BREAKOUT INTO LATITUDINAL BANDS

Latitudinal circles following average frontal location (Orsi et al 1995; Moore et al 1999): SAZ, NPFZ, PF, SPFZ, and SACCF.

REGIONS DEFINED BY FRONTAL POSITIONS



The two December show similar distributions in these bands, but PP was much greater in SPFZ and SACCF in 1999.

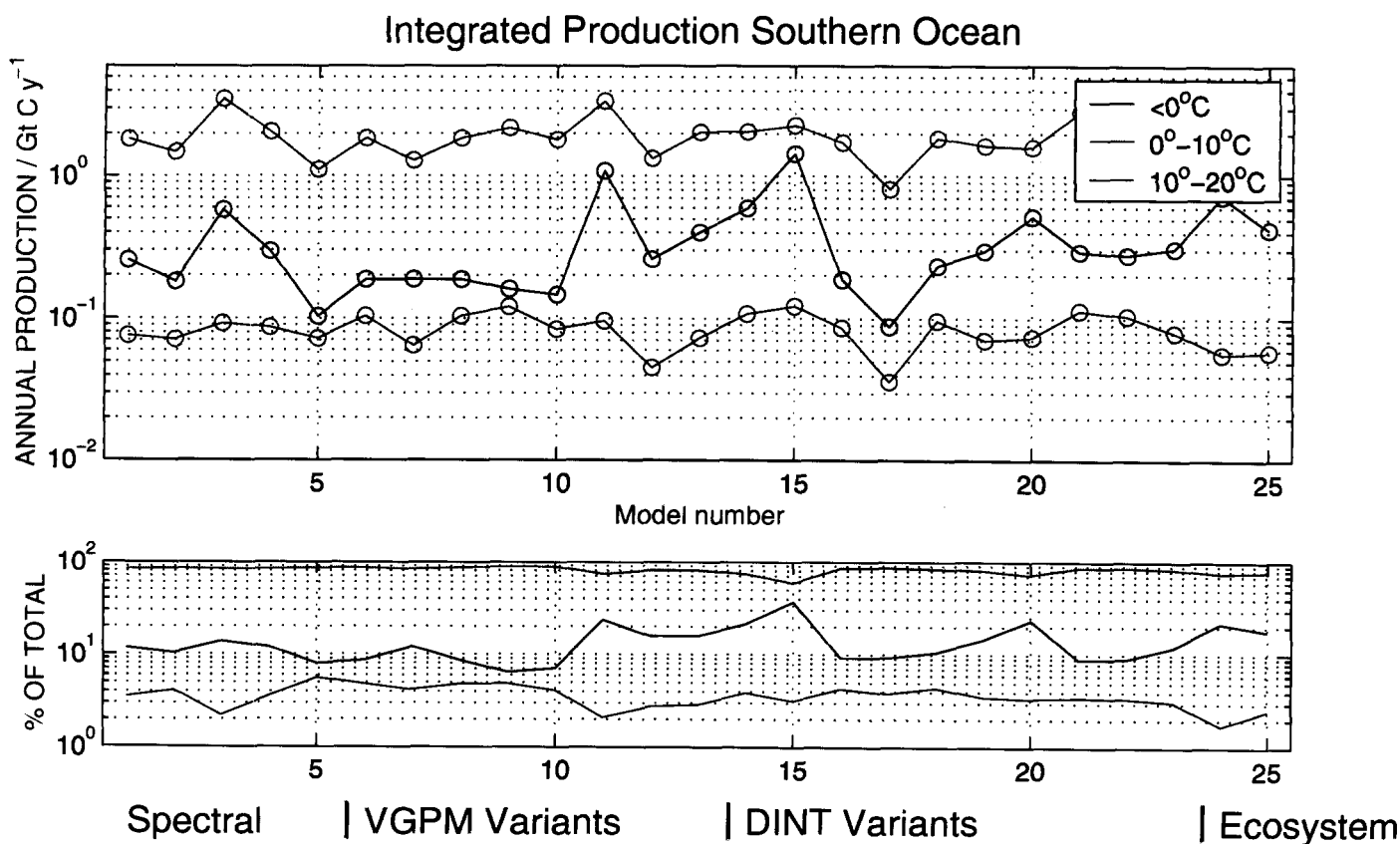


SOUTHERN OCEAN BREAKOUT IN SST LEVELS

LEVEL	AREA	MEAN	MIN	MAX
	% (global%)	Gt C y ⁻¹ (%)		
<0°	20-37 (3)	0.36 (14)	0.004	0.99
0°-10°	60-80 (15)	2.04 (82)	0.12	3.85
10°-20°	0-3 (20)	0.1 (3.9)	0.0002	0.23
> 20°	0 (60)	0	0	0

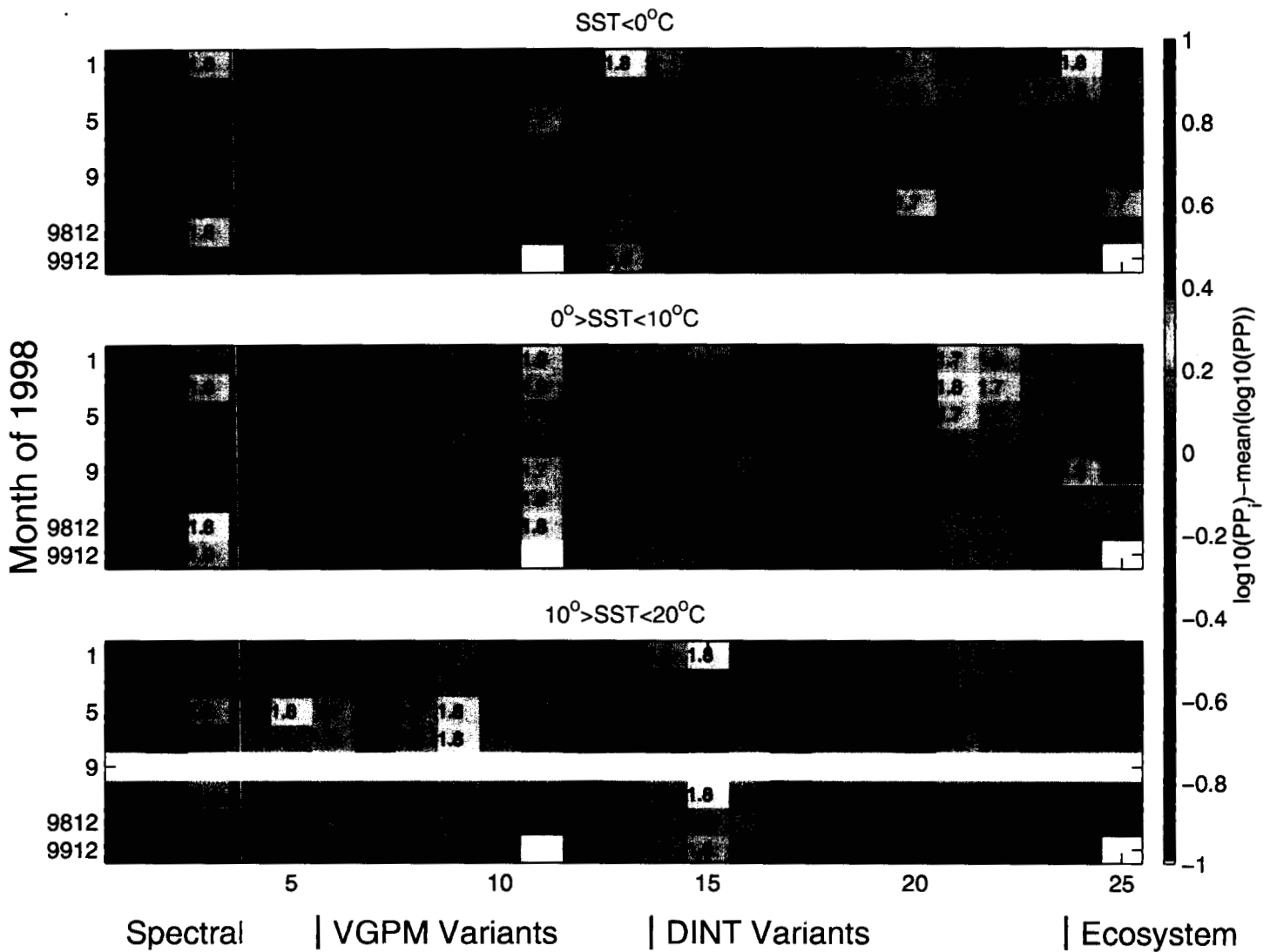
Relative apportioning same in all models.

Most PP is in waters 0-10°C, which may lead to problems with model formulation.



Twelve anomalous models in SST $<0^{\circ}\text{C}$ and about nine in SST $0-10^{\circ}\text{C}$

Some models (e.g. #5 $<10^{\circ}\text{C}$) counter the seasonal cycle, other (e.g. ecosystem) reinforce it.



CONCLUSIONS OF EXAMPLE 2

The spread between models is considerable (almost a factor of 2).

Peak disagreement for *Southern Ocean*, small basins, SST $< 10^{\circ}\text{C}$, and oligotrophic and eutrophic waters.

Generally divergence between models is greater moving south, and for waters $< 10^{\circ}\text{C}$.

We need to use more Southern Ocean data to parameterize the models. Issues such as chlorophyll determination and parameterization of photosynthesis at low SST are likely crucial.

Future work: Uncover the reasons behind these differences (Part 2) and comparison to *in-situ* data (Part 3).

Stay tuned...

Example 3:
NUTRIENT DRAWDOWN AND
AVAILABILITY
FROM SATELLITE ALTIMETER

with O. Sato and P. Polito (INPE, Brasil)

MOTIVATION

Our objective is to obtain a satellite-based estimate of new production from nutrient drawdown that is independent of ocean color and f-ratio determinations.

APPROACH 1:

HEAT STORAGE FROM ALTIMETER

Oceanic heat storage anomaly (HS') is derived from the sea surface height anomaly (η') measured by the TOPEX/Poseidon altimeter (T/P) (Polito *et al.* 2000).

η' is separated into additive components associated with the seasonal cycle, Rossby and Kelvin waves, and mesoscale eddies using a two-dimensional finite impulse response filter.

We use the annual peak-to-peak range in the seasonal non-propagating component of HS' .

Our study period is 1993-2000.

APPROACH 2: NUTRIENT UPTAKE FROM HEAT STORAGE

Changes in HS are inversely related to changes in the storage, NS , of a given nutrient (Nut = nutrient, such as phosphate).

$$NS = \int_{-h}^0 Nut(z) dz, \quad (2)$$

$$NS = a + b * HS, \quad (3)$$

$$NS' = b * HS', \quad (4)$$

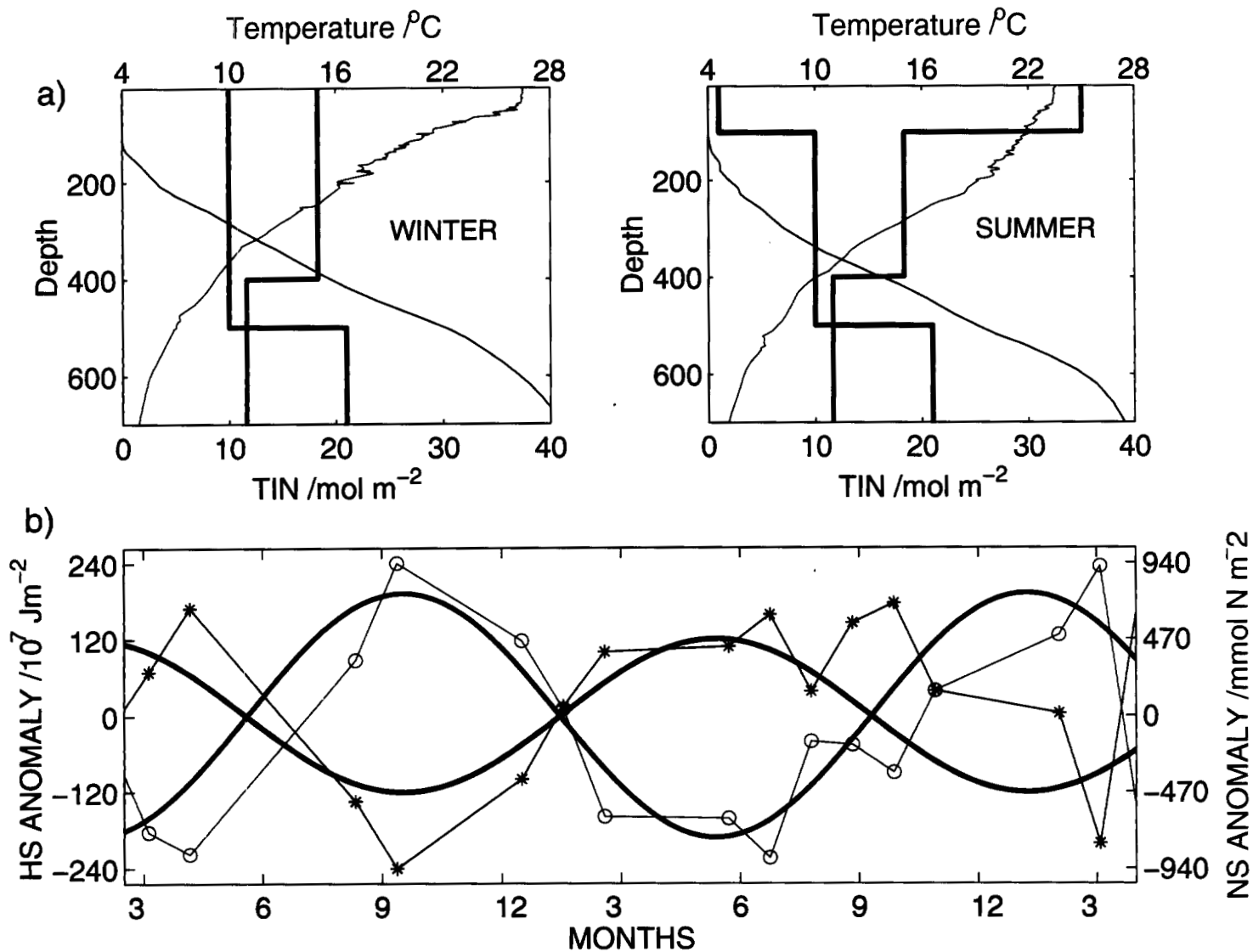
where primed quantities denote the time rate of change, and the slope, b , is a negative number, as high heat content corresponds to low NS .

An increase in HS corresponds to the drawdown (biological uptake) of nutrients, thus a decrease in NS .

When the annual peak-to-peak range in HS is used, the derived NS' is the annual nutrient drawdown.

This method is similar to estimating new production as the product of surface winter nitrate concentration and the depth of the nitrate-depleted upper layer at the end of summer (Strass and Woods 1991).

Idealized profiles (bold) and at the HOT station (thin) of temperature and TIN for winter (April 1993) and summer (September 1993).



Time series of the seasonal anomaly of HS and NS for two years, idealized (bold) and at HOT (thin) from March 1993 to March 1995.

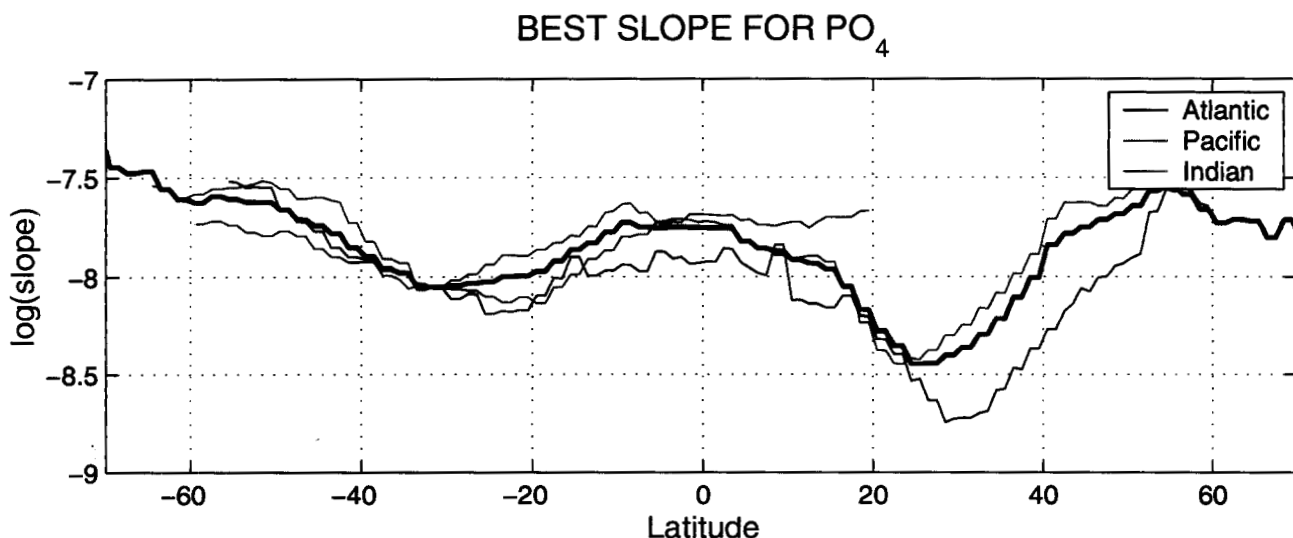
DETERMINATION OF THE SLOPE BETWEEN HS AND NS

We used the monthly climatologies of nutrients (Louanchi and Najjar, 2000), and temperature (World Ocean Atlas, 1998).

The HS and NS were calculated for each depth level.

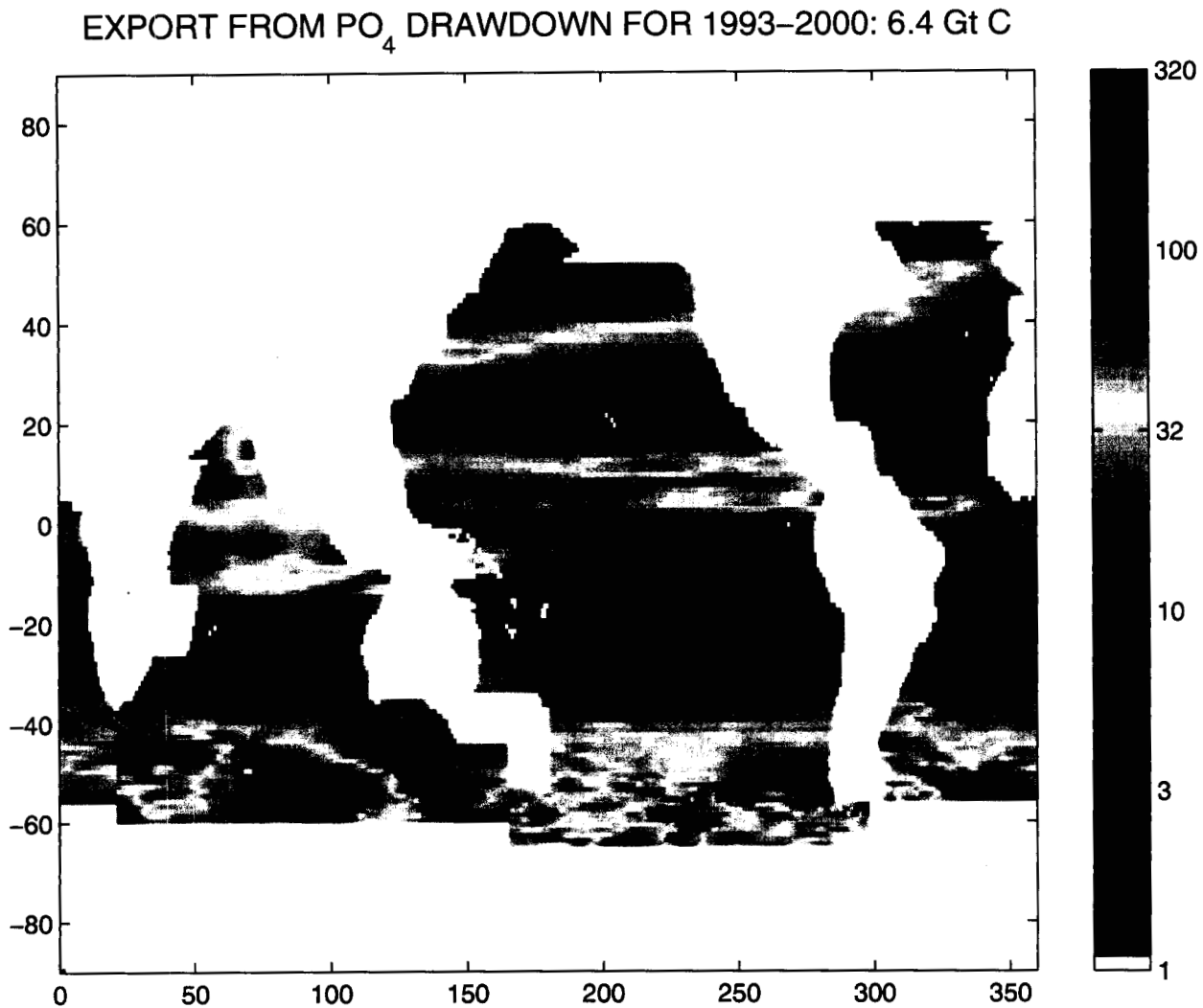
The relationship or slope between time series of HS' and NS' was chosen for the integration level which presented the highest correlation between estimated and observed NS' .

The global slope estimate was zonally averaged for each basin.



GLOBAL NEW PRODUCTION

New production from 1993-2000 from the amplitude of the harmonic fit to the 8-year time series of PO_4 content.



Global new production 6.4 Gt C, is consistent with other estimates.

Export is maximum at high latitude.

REGIONAL NEW PRODUCTION

High latitudes and the Pacific basin present maximum new production (in g C m⁻²).

The subtropical gyres have low new production values (except for the Indian Ocean).

	ATL.	PAC.	IND.	Mean Gt C
>40°N	45 <i>(6)</i>	97 <i>(9)</i>	0 <i>(0)</i>	71 1.2
40-10°N	7 <i>(18)</i>	19 <i>(40)</i>	55 <i>(2)</i>	27 0.95
10°N-10°S	15 <i>(11)</i>	19 <i>(34)</i>	29 <i>(12)</i>	21 1.2
10-40°S	16 <i>(19)</i>	11 <i>(43)</i>	15 <i>(26)</i>	14 1.05
<40°S	44 <i>(10)</i>	34 <i>(21)</i>	38 <i>(22)</i>	39 1.93
Mean Gt C	25 1.3	36 3.4	34 1.7	32 6.4

The number in italics is the area of each region in 10⁶ km².

GLOBAL NEW PRODUCTION FROM CLIMATOLOGY

Annual new production (Gt C) was estimated from the drawdown of nutrients from the climatological data in the upper 125m.

We compare this value with the estimate based on climatological heat storage (in situ) to test the method (Test 1) and with the T/P-based estimate to test its satellite application (Test 2).

IN SITU PO₄	IN SITU HEAT	T/P HEAT
6.7	6.92	6.4

Our estimate of annual new production from the change in nutrient content is in good agreement with the climatological drawdown estimates of Louanchi and Najjar (2000) for the upper 100m (5-6 Gt C).

Test 1: The estimate based on climatological heat storage overestimates the measured drawdown by 3%.

Test 2: The T/P-based estimate underestimates the measured drawdown by 5%.

The difference between the estimate from T/P and from climatological temperature (0.5 Gt C) can be due to interannual variability, or errors associated with ignoring salinity or with using a constant integration depth.

CONCLUSIONS OF EXAMPLE 3

The global new production estimate from T/P altimeter, 6.4 Gt C, is very close to other estimates.

The estimate is within 5-10% of the climatological phosphate drawdown.

The T/P approach yields information about interannual shifts in nutrient availability.

The T/P nutrient storage method, unlike most new production methods, is completely independent of chlorophyll concentration, primary production, or f-ratio measurements, for which we have relatively little data.

An additional advantage over most satellite-based approaches is that it relies on radar altimetry, which is not limited by cloud coverage and already has a relatively long continuous time series (8plus years).

CONCLUSIONS CONCLUSIONS (for real)

- Satellite data can provide invaluable information, otherwise inaccessible.
- Satellite data must be used creatively.
- Satellite data must be used critically.
- New venues for improved oceanographic understanding:
 - as context for in situ surveys
 - to obtain global estimates of critical fluxes